inorganics

MDPI

Review

Cobalt-Based Perovskite Electrodes for Solid Oxide Electrolysis Cells

Chi Zhang [1], Bin Lu [2], Haiji Xiong [2], Chengjun Lin [2], Lin Fang [2], Jile Fu [1,*], Dingrong Deng [2], Xiaohong Fan [2,*], Yi Li [3,*] and Qi-Hui Wu [2]

[1] School of Energy and Chemical Engineering, Xiamen University Malaysia, Jalan Sunsuria, Bandar Sunsuria, Sepang 43900, Malaysia
[2] School of Marine Equipment and Mechanical Engineering, Jimei University, Xiamen 361021, China
[3] Department of Polymer Science and Engineering, College of Chemistry, Chemical Engineering and Materials Science, Soochow University, Suzhou 215123, China
* Correspondence: jile.fu@xmu.edu.my (J.F.); echo_fan@jmu.edu.cn (X.F.); liyi@suda.edu.cn (Y.L.)

Abstract: Recently, many efforts and much attention has been paid to developing environmentally friendly energy. Solid oxide electrolyte cells (SOECs) process in reverse to solid oxide fuel cells (SOFCs) producing hydrogen gas as a green energy source. However, in this application, high-performance catalysts are usually required to overcome the sluggish oxygen evolution reactions (OER) during water decomposition. For this reason, discovery of catalysts with high performance is a crucial issue for the wide application of SOECs. Owning to their inherent activity and adequate stability in electrochemical conditions, perovskite oxides have been intensively employed in SOECs. In this mini review, we summarize the currently available studies concerning the applications of cobalt-based perovskite oxide catalysts in SOECs. Particularly, their structural properties and corresponding electronic structures are discussed based on their electrochemical performance, both experimentally and theoretically.

Keywords: SOEC; cobalt-based perovskite; oxygen evolution reactions; catalyst

Citation: Zhang, C.; Lu, B.; Xiong, H.; Lin, C.; Fang, L.; Fu, J.; Deng, D.; Fan, X.; Li, Y.; Wu, Q.-H. Cobalt-Based Perovskite Electrodes for Solid Oxide Electrolysis Cells. *Inorganics* **2022**, *10*, 187. https://doi.org/10.3390/inorganics10110187

Academic Editor: Chiara Dionigi

Received: 23 September 2022
Accepted: 25 October 2022
Published: 28 October 2022

1. Introduction

In recent years, the methods for hydrogen gas production have attracted much attentions due to the increasing concerns of environmental protection. As the reverse process of solid oxide fuel cells (SOFCs), solid oxide electrolysis cells (SOECs) have been considered as effective devices for hydrogen production with low cost, high efficiency, and environmental friendly [1]. High working temperatures could accelerate the reaction speed in SOECs, thus improving their electrocatalytic capacity [2]. However, even if SOECs take the advantages from elevated temperatures, it is still essential to decrease the working temperatures over long device duration times [3]. However, unfortunately, low working temperatures would also decrease the electrocatalytic activity of the oxygen electrodes and thus result in the degradation of the catalytic performance. Therefore, the development of low-temperature oxygen electrodes with high electrochemical activities is essential research concerning SOECs [4]

Oxygen electrodes applied in SOECs are mainly reference the extensively studied cathodes for SOFCs [5–8]. In SOEC processes, the oxygen evolution reactions (OER) are the most important reactions during water splitting into oxygen and hydrogen gases, in this case, the study of OER, therefore, have become a main topic in the study of hydrogen production in SOECs. Trasatti et al. [9] investigated the OER activities of different perovskite oxides and emphasized a volcano-shaped relationship combining the enthalpy and the corresponding OER overpotential. At the same time, Bockris et al. [10] clarified that the current density at a constant overpotential was contrarily dependent on the formation enthalpy of $M(OH)_3$ hydroxide. The previous activity and mechanism study became

the basis of the subsequent design of efficient oxide electrocatalysts [11]. The perovskite structure, possessing various types of rare/alkaline earth metal cations (A site) and 3D transition-metal cations (M sites), has been reported to exhibit different architectures, some of them possessing diffusion channels for oxygen ions that would be advantageous in the OER process [12]. Partial metal substitution either at A or M sites would significantly influence not only the charge state and distribution of ions in the perovskite structure, but also its electric conductivity, and finally the OER performance [13].

At high temperatures, the defective structure of oxides and their related chemical activities have been extensively detected. $Ln_2NiO_{4-\delta}$ (Ln = Pr, La, Nd) series have been investigated as oxygen electrodes for SOECs [14]. Former data has indicated that $La_2NiO_{4-\delta}$ (LNO) exhibited obvious superiority electrocatalytic activities [15] and performance of surface oxygen exchange [16]. Liu and coworkers confirmed that LNO applied as an SOEC oxygen electrode showed excellent electrochemical catalytic properties [17]. However, former research has also indicated that LNO electrodes would decompose in SOEC operating situations if $Ce_xGd_{1-x}O_{2-\delta}$ (GDC) was used as the oxide electrolyte [18]. This resulted in a rapid degeneracy in performance [16]. Flua's group further proved that the decomposition of LNO on GDC was induced by element diffusion at the LNO–GDC interphase [19]. This decomposition phenomenon was also found at the $La_{0.5}Sr_{0.5}MnO_3$ (LSMO) electrode [20]. The LSMO gradually cracked into nanoparticles due to oxygen ions migrating through the electrolyte during anodic polarization, which led to an alteration in valence of manganese ions and thereafter resulted in lattice shrinkage and consequent breakdown into particles [21,22]. Due to this concern, improved stability of perovskite oxides is a critical point in SOEC research. In addition, although LNO and LSMO have superior performance in oxygen surface exchange [16], they have weakness in electronic conductivity. With the aim to overcome this shortcoming, a $La_2NiO_{4-\delta}$-coated $PrBa_{0.5}Sr_{0.5}Co_{1.5}Fe_{0.5}O_{5-\delta}$ electrode was prepared which showed good electrochemical performances [23,24]. At the same time, $La_{1-x}Sr_xCo_{1-y}Ni_yO_{3-\delta}$ is a common cathode for SOFCs [25,26], moreover, $La_{1-x}Sr_xCo_{1-y}Ni_yO_{3-\delta}$ (LSCNO), $La_{1-x}Sr_xCo_{1-y}Fe_yO_{3-\delta}$ (LSCFO) [27], and $Ba_xSr_{1-x}Co_yFe_{1-y}O_{3-\delta}$ (BSCFO) [28] have also been widely investigated as electrodes for SOECs [29,30]. High electronic conductivity was found for Co-based electrodes [31,32], however this was accompanied by an increasing thermal expansion coefficient [33]. In this case, preparing Co-based perovskites with high thermal stability is a challenge.

Perovskites have been proven to be the one of best cathodes for the SOEC devices, in particular, Co-based ones usually exhibit extremely high catalytic performances due to the multivalent properties of Co ions [34]. In this mini review, the application of Co-based perovskite in hydrogen production in SOEC devices is summarized. The effect of A- and M-site doping and crystal distortion in thin-film structures on OERs is discussed, in addition, the composite perovskite is reviewed providing insights into mending the weakness of single perovskite, and thereafter provide better electrochemical catalysts.

2. Crystal and Electronic Structure of Perovskite Oxides

The crystal structure of perovskite oxide (AMO_3), taking $LaCoO_3$ (LCO) as example, is shown in Figure 1a, which easily describes the prototypical ion-covalent, and the CoO_6 octahedra connected by the corners [35,36]. It features good divisibility in that the A site can be located in any rare-earth or alkaline earth metals, while the M site can be any transition metal, as shown in Figure 1b for the Sr-substituted $LaCoO_3$. In addition, the oxygen stoichiometry can also be varied based on the ratio of different kinds of metal ions. This structural adaptability has been successfully applied to tune the electronic structure of M site cations, specifically recognized as the OER active center, and therefore a target to manipulate the electrocatalytic activities. For example, Cheng and coworkers partially doped Sr^{2+} at the A site in LCO and then obtained increasing activity in OERs, which was attributed to the enhancement in overlap between the unoccupied Co 3d conduction bands and the occupied O 2p valence bands [37]. Zhang et al. replaced Ni with Fe in

$LaNiO_3$ (LNO) to promote its OER activity, resulting from the influence of the Fe doping in strengthening the Ni–O bonding and thus restraining the generation of Ni^{2+} ions on the $LaNi_{1-x}Fe_xO_3$ surface [38]. By employing a reductive heating treatment, Yang et al. produced high oxygen-deficient $CaMnO_{2.5}$, which exhibited great enhancement in OER performance when compared with unreduced $CaMnO_3$. The increase in OER activity was assigned primarily to the propitious electronic configuration of high-spin Mn^{3+} ions induced by sufficient oxygen vacancies in $CaMnO_{2.5}$ [39].

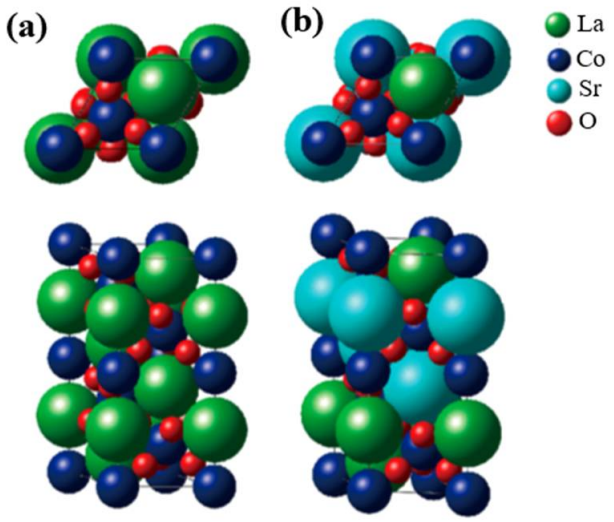

Figure 1. Crystal structure of (**a**) $LaCoO_3$ and (**b**) Sr-doped $LaCoO_3$ ($La_{0.5}Sr_{0.5}CoO_3$). The bulk structure corresponds to the space group rhombohedral R3ch. Derived from [36].

A heterogeneous catalysis greatly relied on the surface electronic structure models associated with the catalytic properties. In this case, the surface oxygen reactivity is thus an important factor for oxidation chemical reactions, such as OERs [40,41]. Due to their excellent flexibility in accepting a high variability of cations in A and/or M locations, the electronic conductivity of perovskites can be manipulated from insulating to metallic. Through careful material design, electronic structures in perovskites can be tailored to the thermodynamic energies of a variety of reactions to minimize electrochemical reaction barriers. Before describing the role of the active sites in OERs, common ideas on the electronic structure of perovskites should be given. The charge transfer energy gained from density functional theory (DFT) calculations has been proven to be the most proper descriptor, which leads to a model of the charge transfer energy between the adsorbates and transition metals (assigned as Δ' in Figure 2). A recently proposed descriptor, charge transfer energy (Δ), displays a linear relationship with the polarization potential (η). This is because that the Δ values are obtained from both theoretical calculations and spectroscopic data. This finding proposes that Δ is the most helpful descriptor in the design of OER perovskite oxide catalysts, as Δ decreases, the Δ' may also decrease and lower the energy. The O 2p band center relative to the Fermi energy and e_g electron number of the transition metal ions at the Msites is not necessarily adequate for the most part of perovskite oxides [42].

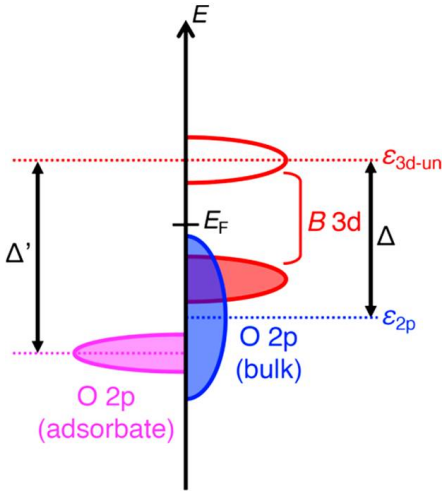

Figure 2. Schematic diagram of the charge transfer energy (Δ) between the catalyst and the adsorbates (Δ′) [42].

3. Co-Based Perovskite for SOECs

3.1. Pure or Doped Perovskite

Co-based perovskite oxides are promising electrocatalysts for OERs applied in various devices; however, a shortage of fundamental comprehension in oxide surfaces obstructs their rational design in order to further enhance their electrochemical performance. In this case, further understanding of the factors which influence OERs is essential. The properties of perovskite electrocatalysts greatly depend on their electronic configurations, especially for electronic conductivity and oxygen vacancy. Figure 3a reports a control method for lattice orientation of LCO films using sol–gel technology, and Figure 3b–d show their corresponding high-resolution transmission electron microscope (HR-TEM) images. The LCO films with different lattice orientations induced different distortion degrees of the CoO_6 octahedron, which results in a spin-state transition of Co ions from a low spin-state ($t_{2g}^6e_g^0$) to an intermediate spin-state ($t_{2g}^5e_g^1$), as proven by the Co L-edge and O K-edge X-ray absorption spectroscopy (XAS). The OER ability of the LCO films has been ascribed to the synergetic effects of the e_g electron filling degree, electronic conductivity, and adsorption free energy of the intermediates. Judging by these descriptions, the LCO(100) film possesses the optimal e_g electron filling degree, which is as high as 0.87, lower adsorption free energy, and higher conductivity as indicated in Figure 4. It shows the best electrocatalytic ability for OERs, which is 2.9 and 6.7 times greater in mass density compared with the LCO(110) and LCO(111) films under an overpotential of 470 mV [43]. This is because that the (100) film appears to possess a JT-like distortion in the CoO_6 octahedrons, consequently elongating the Co–O covalent bonding and thus stabilizing the intermediate spin-state Co^{3+} ($t_{2g}^5e_g^1$) ions. Furthermore, (100) film exposes more Co–O bonds, and the largest tensile extension of Co–O bonds contributes to weakening of the Co–O covalent bonding, which also assists in intermediate adsorption and release of O_2 generated in the electrolyte, empowering a better OER electrocatalytic performance.

Electrochemical studies of the epitaxial $La_{1-x}Sr_xCoO_{3-\delta}$ (LSCO)(001) films have been carried out using in situ and operando ambient pressure X-ray photoelectron spectroscopy (XPS) to detect the effects of surface stoichiometry and electronic structure on OERs. Electrochemical results indicate that both lattice strain and oxygen vacancies play an important role in determining OER performance. In a humid environment, hydroxyl and carbonate affinity increase with Sr content (up to 40%), leading to an increase in the binding energy of metal core levels and the valence band edge, which then induces the formation of a surface dipole. Formation of OH might be impelled by the re-filling of oxygen vacancies and as well as the reduction of Co^{4+} to Co^{3+} ions, as it agrees with the correlation of OH coverage with hole mobility. The combination of in situ and in operando XPS results on

thin films has brought a deeper understanding of the oxide surface and electrochemical interface, which will guide future modeling of the realistic electrocatalyst surfaces and OER mechanisms as well [44].

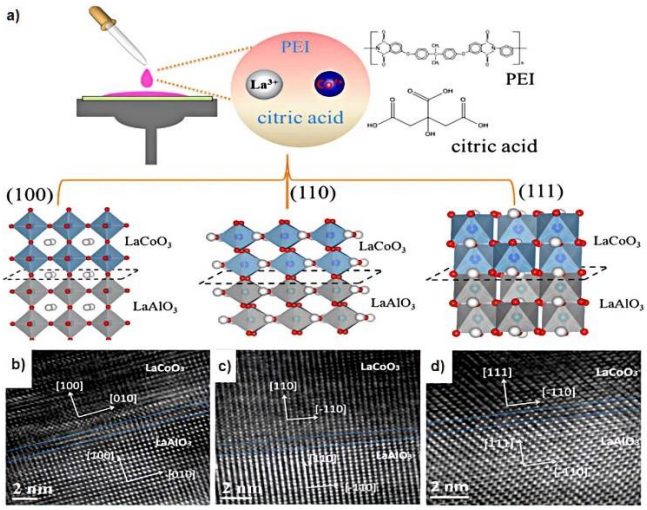

Figure 3. (**a**) Schematic diagram of the preparation process and high-resolution TEM images of the as-prepared (**b**) LCO(100), (**c**) LCO(110), and (**d**) LCO(111) films [43].

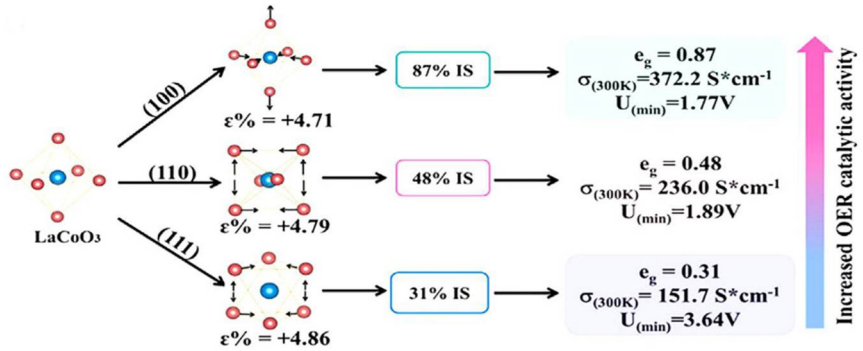

Figure 4. The relationship between OER activity and spin configuration (free energy, conductivity as well as e_g electron filling degree) of the differently oriented LCO films. IS: intermediate spin-state [43].

The effects of lattice strain and oxygen vacancies of oxide catalysts in OERs have been extensively investigated, which are generally treated separately due to the limitations in experimental setup. Recently, the conjugated impacts of both lattice strain and oxygen vacancy on the electrocatalytic activity of LSCO films prepared on the $LaAlO_3$ (LAO) and $SrTiO_3$ (STO) single-crystal substrates have been investigated [45]. Electrochemical experiments showed that the OER activity of the LSCO films was higher under compression rather than under tension and were diminished when oxygen vacancies were introduced. Figure 5 shows the electronic structures of LSCO films with various strain statuses and oxygen deficiencies obtained from the DFT calculations, including density of states (DOS) (Figure 5a), the occupancy of e_g states (Figure 5b), the energy gap between O 2p and Co 3d band center (Δ) (Figure 5c), and oxygen vacancy formation energy on LAO and STO substrates (Figure 5d). Perovskite catalysts with lower Δ values were observed to exhibit greater electronic conductivity and an easier charge transfer process in OERs. A smaller Δ or a higher O 2p band center energy relative to the Fermi level could enhance the participation of lattice oxygen during OERs, thus leading to higher activity. Compared with the effects of strain on the e_g filling degree and Δ value of LSCO for a δ value, the e_g occupancy for LSCO/STO with tensile strain and LSCO/LAO with compressive strain are quite close. Contrarily, the Δ value has proven to be conspicuously greater for LSCO/LAO

than LSCO/STO with same δ, which suggests a lower electronic conductivity, a difficult charge transfer process, and less covalent bonding between metal and oxygen.

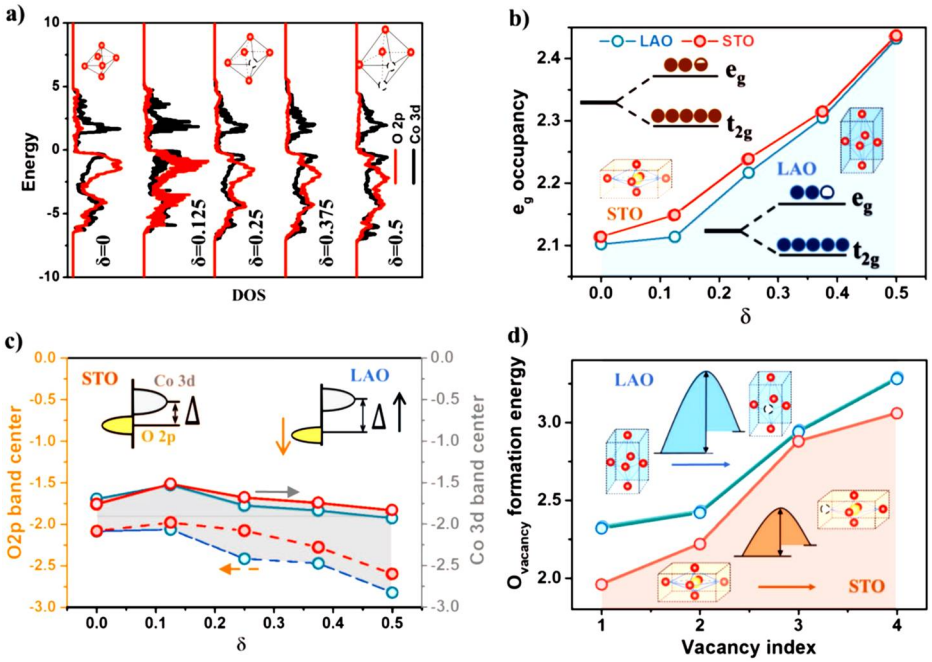

Figure 5. Comparison of electronic properties and oxygen defect formation energy for LSCO/STO and LSC/LAO based on the DFT calculations: (**a**) DOS of the O 2p and Co 3d orbitals for LSCO/LAO against different oxygen deficiency (δ); (**b**) the e_g occupancy for LSCO at different δ values. The inset shows the slightly higher e_g filling degree for LSC/STO; (**c**) the O 2p and Co 3d orbital center for LSCO at various δ values. The inset shows the larger energy gap between O 2p and Co 3d orbitals for LSC/LAO; (**d**) oxygen defect formation energy for LSCO with diver values of oxygen defects for the unit cell. The insets show the minor oxygen defect formation energy for LSC/STO [45].

Such strain induces extra oxygen defects in the LSCO/STO interphase increasing the e_g state filling degree and as well as the energy difference between the O 2p and Co 3d orbitals, resulting in a reduction in OER activity. Both the LSCO/STO and the LSCO/LAO showed inferior OER activities as more oxygen defects are created via vacuum heating treatment. This degradation in OER performance could be reinstated by re-locating oxygen ions back to the films during OER operation. Engineering lattice strain and tuning defect chemistry could be regarded as the effective methods to develop high-performance catalysts. Such regulation could also be applied to other metal oxides and be helpful in piloting the rational design of new kinds of high-performance catalysts for various energy conversion devices. Depending on the calculation results of e_g occupancy and Δ value, one may predict similar or even worse OER activity for LSCO/LAO compared with LSCO/STO if given the same δ value, which in contrast has a noticeably better OER performance for LSCO/LAO than LSCO/STO when observed experimentally. Such alterations in electronic properties are high, possibly due to be the origins of the degraded OER activity for the vacuum-reduced LSCO, observed in electrochemical characterization [45].

Ionic conductor $GdBaCo_2O_{5.5\pm\delta}$ (GBCO) thin film has been grown epitaxially and applied to OERs in electrochemical devices. Time-resolved XRD combined with voltage step chrono-amperometric results provided a deeper understanding of chemical expansion (CE) mechanisms at the GBCO electrode. The CE coefficient at the c-axis showed a negative value during compound oxidation with a remarkable asymmetry from $\alpha_c = -0.037$ to -0.014 at both $\delta < 0$ and $\delta > 0$. This alteration in CE indicated structural changes associated with the alterable Co cation oxidation valence from Co^{2+} to Co^{3+} and then to Co^{4+}. The reaction dynamics gradually decelerated in reduction when $\delta < 0$; however, they still maintained a high catalytic activity when $\delta > 0$, consistent with the structural

variations and the electronic carrier delocalization when crossing δ = 0 [46]. Then, Sr-doped GBCO ($GdBa_{1-x}Sr_xCo_2O_{6-\delta}$, GBSCO) was also investigated, which possesses an enhanced oxygen evolution performance and higher electronic conductivity compared to GBCO. XRD patterns combined with Rietveld analysis indicated that the electrodes with higher Sr-content dopant crystallized with higher tetragonal P4/mmm symmetry. Excellent electrical conductivity of 980 S cm^{-1} was detected for GBSCO, in agreement with the better OER activity at 1.51 V (the onset polarization) versus a reversible hydrogen electrode (RHE). This outstanding electrochemical characteristic was explained based on the wider carrier bandwidth, which is a function of Co–O–Co bending angles and Co–O bonding lengths. Moreover, the higher oxygen evolution activity was observed in spite of the formation of non-lattice oxides and enrichment of alkaline ions at the electrode surface [47]. Thorough understanding of the crystallographic occupancy ordering and surface characteristics are fundamental for optimizing the electronic conductivity, ionic mobility, and electrocatalytic performances, which is critical for designing electrochemical devices with high efficiency.

An easy sol–gel approach was developed to prepare M site ordered double perovskites $Ba_2Bi_xSc_{0.2}Co_{1.8-x}O_{6-\delta}$ (BBSCO), in which Co ions are located in two different environments. The BBSCO electrodes were demonstrated to be superior electrocatalysts for OERs in alkaline solution with long-term test, no obvious performance degradation was observed based in the continuous chronopotentiometry results. The critical role of the ordered [Co^{2+}] and [Sc^{3+}, Bi^{5+}, Co^{3+}] dual environments in improving the OER activity was approved. Compared with BSCFO, the presence of ordered Co dual-site environments explained the high OER activity of BBSCO [48]. A promising Ca-doping method was also used to enhance the durability and electrocatalytic OER activity of $Pr_{0.5}Ba_{0.5}CoO_{3-\delta}$ (PBCO). XRD data indicated that phase structures progressively altered from layered perovskite PBCO to the conventional cubic one with rising Ca content. Compared to pristine PBCO, the electrocatalytic activity of Ca-doped PBCO perovskite was increased by about 90%. More importantly, after one thousand cycles of OER electrolysis tests, the activity of PBCO without Ca doping was degraded by approximately 60%. In contrast, there was almost no activity degradation for the Ca-doped one. These results indicated that the OER durability could be significantly improved by Ca doping, and thus makes it a promising electrocatalyst for electrolysis cells [49].

3.2. Composite Perovskite

Many composite electrodes have been studied as OER catalysts for SOECs, such as LSCFO–$LaSrGaO_4$(LSGO) oxygen electrodes [50], in which LSGO was used as the scaffold, and the LSCFO nanoparticles (~100 nm) were homogeneously coated on to the LSGO scaffold surface. The cathode polarization resistance for the LSCFO–LSGO cathode was lower than that of pure LSCFO. The enhancement in electrochemical performance of the nano-LSCFO–LSGO cathode could be attributed to the improvement of the triple phase boundaries. Qiu and coworkers reported impregnation of LSMO into $Ba_{0.5}Sr_{0.5}Co_{0.8}Fe_{0.2}O_{3-\delta}$ (BSCFO), which greatly improved the CO_2-poisoning resistance of the BSCFO electrodes [36]. The core constituted a porous BSCFO backbone with high oxygen ion conductivity, while the dense shell was composed of LSMO. The presence of the dense LSMO shell prevented the BSCFO core cathode from being poisoned by CO_2, and therefore increased the electrochemical performance of the electrode [51].

By taking advantage of the charge transfer kinetics at the junction of RuO_2/LBSCFO perovskite, the SOEC demonstrated an outstanding electrochemical performance [52], which delivered a current density of ~2.26 A cm^{-2} at 1.6 V and 600 °C, and was maintained after 90 h. The built-in charge transfer in the RuO_2/LBSCFO junction revealed the electron donation from the Co–O bonding orbitals to the RuO_2 clusters. In addition, RuO_2 further reinforced the electrocatalytic performance by enhancing the mass transport during OERs. Sharma and coworkers studied Cr deposition on LSCO as the contact layer [53], and concluded that Cr deposition occurred throughout the whole LSCO contact layer after polarization at SOEC conditions for 2000 h by the formation of La–Cr–O phases at the elec-

trode's outermost surface. Later on, the influence of Cr deposition on the electrochemical activity of LSCFO electrodes under SOEC operating conditions was also investigated [54]. The formation of a major $SrCrO_4$ phase on the LSCFO surface and rapid degradation in the electrochemical activity were observed. Fabrication of perovskite oxide with various carbon materials to form composite catalysts is a widely accepted strategy to improve OER catalytic activities. Porous $Sm_{0.5}Sr_{0.5}CoO_{3-\delta}$ (SSCO) hollow nanofibers composited with cross-linked, three-dimensional, and N-doped graphene [55] exhibited a remarkable enhancement in OER activity in alkaline media. The onset potential for OERs is only 1.53 V with a Tafel slope of 115 mV dec^{-1}. The synergistic effect between SSCO and graphene components in the OER process were revealed by the DFT calculations, which suggested that the electron transport from graphene to O_2 and SSCO enhanced the electrocatalytic reaction activity by activating the O_2 via increasing the covalent bonding of lattice oxygen. The significance of this result suggests a direction for the design of perovskite-type bifunctional catalysts to improve OERs.

4. Conclusions & Perspective

Co-based perovskites applied in SOECs has been reviewed. The previous research data indicated that the excellent electrochemical properties of Co-based perovskites in hydrogen production strongly depend on their electronic and crystal structures. In addition, the solid interface would also enhance the catalytic capability by increasing the electron transport. The previous reports indicated that an enhancement in the transport properties is usually linked to an increasing mismatch in the thermal expansion; therefore, the suitable design of a Co-based perovskite is important. There is a common way to limit the thermal expansion of Co-based perovskite by surface coating of ceria-based oxide or impregnating them into LNO, which is an impactful way to design high-performance SOEC cathodes. The electronic structural design could be realized from the chemical flexibility of perovskites by replacing or partial replacing A and/or M metals. Moreover, the different crystal structures of a perovskite could be prepared on different substrates, and then exhibit various electronic properties which could influence the OER process. The literature data indicates that surface and interfacial engineering by altering the crystal strain and heterointerfaces presents exciting opportunities to enhance the electrocatalytic properties of perovskites.

We mainly have two perspectives for future research. First, to draw a reliable picture concerning the impacts of lattice strain, surface electronic and crystal structures on OER activity, which is necessary to combine advanced theoretical calculations and experimental research. The results obtained, both theoretically and experimentally, could be used to better understand the role of surface and interfacial engineering on the design of proper perovskites for OERs. Based on this understanding, one can rationally design an electrocatalyst with high activity and stability for different applications. Secondly, besides the activity, the long-term stability of oxide catalysts is also essential for the practical application of oxide catalysts. To understand the reasons of performance reduction with time, in situ characterization techniques are essential to gain valuable information on trancing the material properties under real operating conditions. The in situ measurement results during electrochemical tests will provide useful information, beneficial to the rational design of catalysts with high activity. In this case, developing new in situ techniques to monitor true catalysts with a combination of theoretical calculations would make it possible to determine OER active sites and comprehensively understand the OER mechanism. This would facilitate the design of high-efficiency and robust OER catalysts which could be applied in high-performance SOECs.

Author Contributions: Conceptualization, Q.-H.W., J.F., X.F. and Y.L.; methodology, D.D.; formal analysis, B.L. and L.F.; investigation, C.Z.; data curation, C.Z., H.X. and C.L.; writing—original draft preparation, C.Z.; writing—review and editing, Q.-H.W. and J.F.; funding acquisition, Q.-H.W. All authors have read and agreed to the published version of the manuscript.

Funding: This research was funded by the Starting Research Fund from Jimei University and Xiamen University Malaysia.

Conflicts of Interest: The authors declare no conflict of interest.

References

1. Tucker, M.C. Progress in metal-supported solid oxide electrolysis cells: A review. *Int. J. Hydrogen Energy* **2020**, *45*, 24203–24218. [CrossRef]
2. Ni, M.; Leung, M.K.H.; Leung, D.Y.C. Technological development of hydrogen production by solid oxide electrolyzer cell (SOEC). *Int. J. Hydrogen Energy* **2008**, *33*, 2337–2354. [CrossRef]
3. Gaudillere, C.; Navarrete, L.; Serra, J.M. Syngas production at intermediate temperature through H_2O and CO_2 electrolysis with a Cu-based solid oxide electrolyzer cell. *Int. J. Hydrogen Energy* **2014**, *39*, 3047–3054. [CrossRef]
4. Buttler, A.; Hartmut, S. Current status of water electrolysis for energy storage, grid balancing and sector coupling via power-to-gas and power-to-liquids: A review. Renew. *Sustain. Energy Rev.* **2018**, *82*, 2440–2454. [CrossRef]
5. Zheng, Y.; Wang, J.; Yu, B.; Zhang, W.; Chen, J.; Qiao, J.; Zhang, J. A review of high temperature co-electrolysis of H_2O and CO_2 to produce sustainable fuels using solid oxide electrolysis cells (SOECs): Advanced materials and technology. *Chem. Soc. Rev.* **2017**, *46*, 1427–1463. [CrossRef] [PubMed]
6. Ritucci, H.; Agersted, K.; Zielke, P.; Wulff, A.C.; Khajavi, P.; Smeacetto, F.; Sabato, A.G.; Kiebach, R. A Ba-free sealing glass with a high coefficient of thermal expansion and excellent interface stability optimized for SOFC/SOEC stack applications. *Int. J. Appl. Ceram. Technol.* **2018**, *15*, 1011–1022. [CrossRef]
7. Hou, Y.; Wang, L.; Bian, L.; Wang, Y.; Chou, K.C. Excellent electrochemical performance of $La_{0.3}Sr_{0.7}Fe_{0.9}Ti_{0.1}O_{3-\delta}$ as a symmetric electrode for solid oxide cells. *ACS Appl. Mater. Interfaces* **2021**, *13*, 22381–22390.
8. Li, P.; Xuan, Y.; Jiang, B.; Zhang, S.; Xia, C. Hollow $La_{0.6}Sr_{0.4}Ni_{0.2}Fe_{0.75}Mo_{0.05}O_{3-\delta}$ electrodes with exsolved $FeNi_3$ in quasi-symmetrical solid oxide electrolysis cells for direct CO_2 electrolysis. *Electrochem. Commun.* **2022**, *134*, 107188. [CrossRef]
9. Trasatti, S. Electrocatalysis by oxides-Attempt at a unifying approach. *Electroanal. Chem. Interfacial Electrochem.* **1980**, *111*, 125–131. [CrossRef]
10. Otagawa, T.; Bockris, J.O. Oxygen evolution on perovskites. *J. Phys. Chem.* **1983**, *87*, 2960–2971.
11. Gupta, S.; Kellogg, W.; Xu, H.; Liu, X.; Cho, J.; Wu, G. Bifunctional perovskite oxide catalysts for oxygen reduction and evolution in alkaline media. *Chem. Asian J.* **2016**, *11*, 10–21. [CrossRef] [PubMed]
12. Han, P.; Jin, K.J.; Lu, H.B.; Jia, J.F.; Qiu, J.; Hu, C.L.; Zhen, G.Z. Influence of oxygen vacancy on transport property of perovskite oxide heterostructures. *Chin. Phys. Lett.* **2009**, *26*, 027301.
13. Lu, C.H.; Biesold-McGee, G.V.; Liu, Y.; Kang, Z.; Lin, Z. Doping and ion substitution in colloidal metal halide perovskite nanoscrystals. *Chem. Soc. Rev.* **2020**, *49*, 4953–5007. [CrossRef] [PubMed]
14. Laguna-Bercero, M.A.; Monzon, H.; Larrea, A.; Orera, V.M. Improved stability of reversible solid oxide cells with a nickelate-based oxygen electrode. *J. Mater. Chem.* **2016**, *4*, 1446–1453. [CrossRef]
15. Lee, Y.; Kim, H. Electrochemical performance of $La_2NiO_{4-\delta}$ cathode for intermediate-temperature solid oxide fuel cells. *Ceram. Int.* **2015**, *41*, 5984–5991. [CrossRef]
16. Tong, X.; Zhou, F.; Yang, S.; Zhong, S.; Wei, M.; Liu, Y. Performance and stability of Ruddlesden-Popper $La_2NiO_{4-\delta}$ oxygen electrodes under solid oxide electrolysis cell operation conditions. *Ceram. Int.* **2017**, *43*, 10927–10933. [CrossRef]
17. Kim, S.J.; Kim, K.J.; Dayaghi, A.M.; Choi, G.M. Polarization and stability of $La_2NiO_{4-\delta}$ in comparison with $La_{0.6}Sr_{0.4}Co_{0.2}Fe_{0.8}O_{3-\delta}$ as air electrode of solid oxide electrolysis cell. *Int. J. Hydrogen Energy* **2016**, *41*, 14498–14506. [CrossRef]
18. Spiridigliozzi, L.; Di Bartolomeo, E.; Dell'Agli, G. Zurlo, F. GDC-based infiltrated electrodes for solid oxide electrolyzer cells (SOECs). *Appl. Sci.* **2020**, *10*, 3882. [CrossRef]
19. Flura, A.; Nicollet, C.; Vibhu, V.; Zeimetz, B.; Rougier, A.; Bassat, J.-M.; Grenier, J.-C. Application of the Adler-Lane-Steele model to porous $La_2NiO_{4-\delta}$ SOFCcathode: Influence of interfaces with gadolinia doped ceria. *J. Electrochem. Soc.* **2016**, *163*, F523–F532. [CrossRef]
20. Liu, H.; Qi, J.; Feng, M.; Xu, H.; Liu, R.; Li, N.; Wang, C.; Zhang, Y.; Zhang, Y.; Lu, W. The tunability of oxygen evolution reaction in flexible van der Waals manganite membrane. *Adv. Sustain. Sys.* **2021**, *5*, 2100073. [CrossRef]
21. Huang, M.; Jiang, H.; Liu, X.; Xiao, Y.; Kong, J.; Zhou, T. LSCM-GDC as composite cathodes for high temperature steam electrolysis: Performance optimization by composition and microstructure tailoring. *Int. J. Hydrogen Energy* **2022**, *47*, 34784–34793. [CrossRef]
22. Busse, P.; Yin, Z.; Mierwaldt, D.; Scholz, J.; Kressdorf, B.; Glaser, L.; Miedema, P.S.; Rothkirch, A.; Viefhaus, J.; Jooss, C.; et al. Probing the surface of $La_{0.6}Sr_{0.4}MnO_3$ in water vapor by in situ photo-in/photon-out spectroscopy. *J. Phys. Chem. C* **2020**, *124*, 7893–7902. [CrossRef]
23. Li, J.; Qiu, P.; Xia, M.; Jia, L.; Chi, B.; Pu, J.; Li, J. Microstructure optimization for high performance $PrBa_{0.5}Sr_{0.5}Co_{1.5}Fe_{0.5}O_{5-\delta}$-$La_2NiO_{4-\delta}$ core-shell cathode of solid oxide fuel cells. *J. Power Sources* **2018**, *379*, 206–211. [CrossRef]
24. Li, J.; Zhang, Q.; Qiu, P.; Jia, L.; Chi, B.; Pu, J.; Li, J. A CO_2-tolerant $La_2NiO_{4-\delta}$-coated $PrBa_{0.5}Sr_{0.5}Co_{1.5}Fe_{0.5}O_{5-\delta}$ cathode for intermediate temperature solid oxide fuel cells. *J. Power Sources* **2017**, *342*, 623–628. [CrossRef]

25. Hjalmarsson, P.; Sogaard, M.; Mogensen, M. Electrochemical behaviour of $(La_{1-x}Sr_x)_sCo_{1-y}Ni_yO_{3-\delta}$ as porous SOFC cathodes. *Solid State Ionics* **2009**, *180*, 1395–1405. [CrossRef]
26. Chen, J.; Liang, F.L.; Liu, L.; Jiang, S.P.; Li, J. Characterization and evaluation of $La_{0.8}Sr_{0.2}Co_{0.8}Ni_{0.2}O_{3-\delta}$ prepared by a polymer-assisted combustion synthesis as a cathode material for intermediate temperature solid oxide fuel cells. *Int. J. Hydrogen Energy* **2009**, *34*, 6845–6851. [CrossRef]
27. Ai, N.; He, S.; Li, N.; Zhang, Q.; Rickard, W.D.A.; Chen, K.; Zhang, T.; Jiang, S.P. Suppressed Sr segregation and performance of directly assembled $La_{0.6}Sr_{0.4}Co_{0.2}Fe_{0.8}O_{3-\delta}$ oxygen electrode on Y_2O_3-ZrO_2 electrolyte of solid oxide electrolysis cells. *J. Power Sources* **2018**, *384*, 125–135. [CrossRef]
28. Qiu, P.; Wang, A.; Li, J.; Li, Z.; Jia, L.; Chi, B.; Pu, J.; Li, J. Promoted CO_2-poisoningresistance of $La_{0.8}Sr_{0.2}MnO_{3-\delta}$-coated $Ba_{0.5}Sr_{0.5}Co_{0.8}Fe_{0.2}O_{3-\delta}$ cathode for intermediate temperature solid oxide fuel cells. *J. Power Sources* **2016**, *327*, 408–413. [CrossRef]
29. Tan, Y.; Duan, N.; Wang, A.; Yan, D.; Chi, B.; Wang, N.; Pu, J.; Li, J. Performance enhancement of solution impregnated nanostructured $La_{0.8}Sr_{0.2}Co_{0.8}Ni_{0.2}O_{3-\delta}$ oxygen electrode for intermediate temperature solid oxide electrolysis cells. *J. Power Sources* **2016**, *305*, 168–174. [CrossRef]
30. Zheng, H.; Tian, Y.; Zhang, L.; Chi, B.; Pu, J.; Jian, L. $La_{0.8}Sr_{0.2}Co_{0.8}Ni_{0.2}O_{3-\delta}$ impregnated oxygen electrode for H_2O/CO_2 co-electrolysis in solid oxide electrolysis cells. *J. Power Sources* **2018**, *383*, 93–101. [CrossRef]
31. Liu, Y.; Chen, J.; Liang, F.; Pu, J.; Chi, B.; Jian, L. Thermochemical compatibility and polarization behaviors of $La_{0.8}Sr_{0.2}Co_{0.8}Ni_{0.2}O_{3-\delta}$ as a cathode material for solid oxide fuel cell. *Int. J. Hydrogen Energy* **2013**, *38*, 6802–6808. [CrossRef]
32. Sun, C.; Alonso, J.A.; Bian, J. Recent advances in perovskite-type oxides for energy conversion and storage applications. *Adv. Energy Mater.* **2020**, *11*, 2000459. [CrossRef]
33. van Doorn, R.H.E.; Bouwmeester, H.J.M.; Burggraaf, A.J. Kinetic decomposition of $La_{0.3}Sr_{0.7}CoO_{3-\delta}$ perovskite membranes during oxygen permeation. *Solid State Ionics* **1998**, *111*, 263–272. [CrossRef]
34. Simböck, J.; Ghiasi, M.; Schönebaum, S.; Simon, U.; de Groot, F.M.F.; Palkovits, R. Electronic parameters in cobalt-based perovskite-type oxides as descriptors for chemocatalytic reactions. *Nat. Commun.* **2020**, *11*, 652. [CrossRef] [PubMed]
35. Hwang, J.; Rao, R.R.; Giordano, L.; Katayama, Y.; Yu, Y.; Shao-Horn, Y. Perovskites in catalysis and electrocatalysis. *Science* **2017**, *358*, 751–756. [CrossRef]
36. Seo, M.H.; Park, H.W.; Lee, D.U.; Park, M.G.; Chen, Z. Design of highly active perovskite oxides for oxygen evolution reaction by combining experimental and ab initio studies. *ACS Catal.* **2015**, *5*, 4337–4344. [CrossRef]
37. Cheng, Y.; Raman, A.S.; Paige, J.; Zhang, L.; Sun, D.; Chen, M.U.; Vojvodic, A.; Gorte, R.J.; Vohs, J.M. Enhancing oxygen exchange activity by tailoring perovskite surfaces. *J. Phys. Chem. Lett.* **2019**, *10*, 4082–4088. [CrossRef]
38. Zhang, D.; Song, Y.; Du, Z.; Wang, L.; Li, Y.; Goodenough, J.B. Active $LaNi_{1-x}Fe_xO_3$ bifunctional catalysts for cathodes in alkaline media. *J. Mater. Chem. A* **2015**, *3*, 9421–9426. [CrossRef]
39. Kim, J.; Chen, X.; Pan, Y.; Shih, P.; Yang, H. W-doped $CaMnO_{2.5}$ and $CaMnO_3$ electrocatalysts for enhanced performance in oxygen evolution and reduction reactions. *J. Electrochem. Soc.* **2017**, *164*, F1074–F1080. [CrossRef]
40. Dickens, C.F.; Montoya, J.H.; Kulkarni, A.R.; Bajdich, M.; Norskov, J.K. An electronic structure descriptor for oxygen reactivity at metal and metal-oxide surfaces. *Surf. Sci.* **2019**, *681*, 122–129. [CrossRef]
41. Suntivich, J.; May, K.J.; Gasteiger, H.A.; Goodenough, J.B.; Shao-Horn, Y. A perovskite oxide optimized for oxygen evolution catalysis from molecular orbital principles. *Science* **2011**, *334*, 1383–1385. [CrossRef] [PubMed]
42. Yamada, I.; Takamatsu, A.; Asai, K.; Shirakawa, T.; Ohzuku, H.; Seno, A.; Uchimura, T.; Fujii, H.; Kawaguchi, S.; Wada, K.; et al. Systematic study of descriptors for oxygen evolution reaction catalysis in perovskite oxides. *J. Phys. Chem. C* **2018**, *122*, 27885–27892. [CrossRef]
43. Tong, Y.; Guo, Y.; Chen, P.; Liu, H.; Zhang, M.; Zhang, L.; Yan, W.; Chu, W.; Wu, C.; Xie, Y. Spin-state regulation of perovskite cobaltite to realize enhanced oxygen evolution activity. *Chem* **2017**, *3*, 812–821. [CrossRef]
44. Stoerzinger, K.A.; Wang, X.R.; Hwang, J.; Rao, R.R.; Hong, W.T.; Rouleau, C.M.; Lee, D.; Yu, Y.; Crumlin, E.J.; Shao-Horn, Y. Speciation and electronic structure of $La_{1-x}Sr_xCoO_{3-\delta}$ during oxygen electrolysis. *Top. Catal.* **2018**, *61*, 2161–2174. [CrossRef]
45. Liu, X.; Zhang, L.; Zheng, Y.; Guo, Z.; Zhu, Y.; Chen, H.; Li, F.; Liu, P.; Yu, B.; Wang, X.; et al. Uncovering the effect of lattice strain and oxygen deficiency on electrocatalytic activity of perovskite cobaltite thin films. *Adv. Sci.* **2019**, *6*, 1801898. [CrossRef]
46. Chatterjee, A.; Caicedo, J.M.; Ballesteros, B.; Santiso, J. $GdBaCo_2O_{5.5}$ electrodes in a solid-state electrochemical cell by time-resolved X-ray diffraction. *J. Mater. Chem. A* **2018**, *6*, 12430–12439. [CrossRef]
47. Pramana, S.S.; Cavallaro, A.; Li, C.; Handoko, A.D.; Chan, K.W.; Walker, R.J.; Regoutz, A.; Herrin, J.S.; Yeo, B.S.; Payne, D.J.; et al. Crystal structure and surface characteristic of Sr-doped $GdBaCo_2O_{6-\delta}$ double perovskites: Oxygen evolution reaction and conductivity. *J. Mater. Chem. A* **2018**, *6*, 5335–5345. [CrossRef]
48. Sun, H.; Chen, G.; Zhu, Y.; Liu, B.; Zhou, W.; Shao, Z. B-site cation ordered double perovskites as efficient and stable electrocatalysts for oxygen evolution reaction. *Chem. Eur. J.* **2017**, *23*, 5722–5728. [CrossRef]
49. He, D.; He, G.; Jiang, H.; Chen, Z.; Huang, M. Enhanced durability and activity of the perovskite electrocatalyst $Pr_{0.5}Ba_{0.5}CoO_{3-\delta}$ by Ca doping for the oxygen evolution reaction at room temperature. *Chem. Commun.* **2017**, *53*, 5132–5135. [CrossRef]
50. Yoon, B.Y.; Bae, J. Characteristics of nano $La_{0.6}Sr_{0.4}Co_{0.2}Fe_{0.8}O_{3-\delta}$-infiltrated $La_{0.8}Sr_{0.2}Ga_{0.8}Mg_{0.2}O_{3-\delta}$ scaffold cathode for enhanced oxygen reduction. *Int. J. Hydrogen Energy* **2013**, *38*, 13399–13407. [CrossRef]

51. Risck, M.; Stoerzinger, K.A.; Maruyama, S.; Hong, W.T.; Takeuchi, I.; Shao-Horn, Y. $La_{0.8}Sr_{0.2}MnO_{3-\delta}$ decorated with $Ba_{0.5}Sr_{0.5}Co_{0.3}Fe_{0.2}O_{3-\delta}$: A bifunctional surface for oxygen electrocatalysis with enhanced stability and activity. *J. Am. Chem. Soc.* **2014**, *136*, 5229–5232.
52. Li, M.; Hua, B.; Chen, J.; Zhong, Y.; Luo, J.-L. Charge transfer dynamics in RuO_2/perovskite nanohybrid for enhanced electrocatalysis in solid oxide electrolyzers. *Nano Energy* **2019**, *57*, 186–194. [CrossRef]
53. Sharma, V.I.; Yildiz, B. Degradation mechanism in $La_{0.8}Sr_{0.2}CoO_3$ as contact layer on the solid oxide electrolysis cell anode. *J. Electrochem. Soc.* **2010**, *157*, B441–B448. [CrossRef]
54. Wei, B.; Chen, K.F.; Zhao, L.; Lu, Z.; Jiang, S.P. Chromium deposition and poisoning at $La_{0.6}Sr_{0.4}Co_{0.2}Fe_{0.8}O_{3-\delta}$ oxygen electrodes of solid oxide electrolysis cells. *Phys. Chem. Chem. Phys.* **2015**, *17*, 1601–1609. [CrossRef] [PubMed]
55. Bu, Y.; Nam, G.; Kim, S.; Choi, K.; Zhong, Q.; Lee, J.; Qin, Y.; Cho, J.; Kim, G. A tailored bifunctional electrocatalyst: Boosting oxygen reduction/evolution catalysis via electron transfer between N-doped graphene and perovskite oxides. *Small* **2018**, *14*, 1802767. [CrossRef]